ACADEMIC PRESS

Available online at www.sciencedirect.com
SCIENCE DIRECT®

NeuroImage

NeuroImage 20 (2003) 1591–1600

www.elsevier.com/locate/ynimg

In vivo tracing of major rat brain pathways using manganese-enhanced magnetic resonance imaging and three-dimensional digital atlasing

Trygve B. Leergaard,[a,b] Jan G. Bjaalie,[a] Anna Devor,[b] Lawrence L. Wald,[b] and Anders M. Dale[b,*]

[a] *Neural Systems and Graphics Computing Laboratory, Centre for Molecular Biology and Neuroscience & Department of Anatomy, Institute of Basic Medical Sciences, University of Oslo, N-0317 Oslo, Norway*

[b] *Massachusetts General Hospital, Nuclear Magnetic Resonance Center, Building 149, 13th Street, Charlestown, MA 02129, USA*

Received 12 March 2003; revised 18 July 2003; accepted 22 July 2003

Abstract

The magnetic resonance imaging (MRI)-detectable T_1 contrast agent manganese (Mn^{2+}) has recently been introduced as a neural tracer in rodents, birds, and monkeys. We have tested to what extent this in vivo method is useful for three-dimensional (3-D) survey of connectivity patterns in the rat somatosensory system. A commonly available 3 T human clinical MRI scanner was used to trace neural pathways following focal injection of manganese chloride ($MnCl_2$) in the somatosensory cortex. Six to 10 h after $MnCl_2$ injection, we found significant signal enhancement in major projection systems, including corticocortical, corticostriatal, corticothalamic, corticotectal, corticopontine, and corticospinal pathways. To facilitate the assignment of anatomic localization to the observed Mn^{2+} signal enhancement, we registered the MRI data with a 3-D digital reconstruction of a stereotaxic rat brain atlas. Across-animal comparison using the digital model allowed demonstration of a corticothalamic 3-D topographic organization in agreement with previously published two-dimensional topographic schemes based on classical neural tracing data. We conclude that anterograde $MnCl_2$/MRI tracing allows rapid analysis of topographic organization across multiple brain regions. The method allows a higher data throughput for 3-D studies of large-scale brain connectivity than conventional methods based on tissue sectioning.

Keywords: Brain atlas; Corticocortical; Cortico-subcortical; Corticothalamic; Neural tracing; T_1-weighted MRI; Topography

Introduction

Functional understanding of the brain critically depends on knowledge about the existence of connections between specific parts of the brain and the architecture of neural circuitry under normal and pathological conditions (for a review of classical literature, see Brodal, 1981). Several thousand experimental investigations, using degeneration methods and neural tracing techniques (see, e.g., Cowan and Cuénod, 1975; Mesulam, 1982; Heimer and Zaborszky, 1989; Köbbert et al., 2000; Lanciego and Wouterlood, 2000), have contributed valuable descriptions of connectivity in the mammalian brain. Most of these investigations have focused on only a limited number of circuits at a time. There are few or virtually no studies that provide descriptions of the complete, large-scale three-dimensional (3-D) circuitry for a given brain region.

Tomographic imaging methods provide new opportunities for in vivo mapping of brain circuitry. The use of the paramagnetic contrast agent manganese ($MnCl_2$) for magnetic resonance imaging (MRI)-based tracing of neural pathways was introduced by Pautler et al. (1998). The method has been applied in the rodent olfactory and visual systems (Pautler et al., 1998; Lin et al., 2001; Watanabe et al., 2001; Natt et al., 2002; Pautler and Koretsky, 2002) in the primate basal ganglia (Saleem et al., 2002), as well as in the vocal system of birds (Van der Linden et al., 2002). The specificity of anterograde Mn^{2+} transport has been demonstrated by combined $MnCl_2$ and wheat germ agglutinin–

* Corresponding author. Fax: +1-617-726-7422.
E-mail address: dale@nmr.mgh.harvard.edu (A.M. Dale).

1053-8119/$ – see front matter © 2003 Elsevier Inc. All rights reserved.
doi:10.1016/S1053-8119(03)00459-2

horseradish peroxidase tracing (Saleem et al., 2002). In contrast to conventional histological techniques, the $MnCl_2$/MRI method allows longitudinal studies in individual animals submitted to external perturbations (discussed in Pautler and Koretsky, 2002; Saleem et al., 2002; Van der Linden et al., 2002). The method allows direct acquisition of three-dimensional distribution data from whole-brain image volumes (for discussion of tomographic methods, see Toga and Mazziotta, 2000, 2002), bypassing the need for elaborate data acquisition and 3-D reconstruction from large numbers of serial sections (Leergaard and Bjaalie, 2002). It is, however, uncertain whether the method is sufficiently sensitive to visualize complete projections from a cortical area onto other parts of the cortex, and simultaneously onto subcortical levels. Further, it is not known whether the 3-D topographic organization within a given projection can be revealed. Finally, in relation to overall mapping of projections and topography within projections, digital atlasing approaches for assigning localization to $MnCl_2$/MRI tracing results need to tested and validated.

In the present study we have tested the capability of the method to label multiple corticocortical and cortico-subcortical projection systems in the same animal, as well as its potential for revealing 3-D topography with across animal comparison. We explored the value of linear normalization techniques for obtaining spatial registration between a 3-D anatomic atlas and the MRI volumes recorded from different animals subjected to $MnCl_2$ tracer injections. $MnCl_2$ was injected in the somatosensory cortex of rats and the ensuing labeling in major brain structures was mapped with use of 3 T human clinical MRI scanner. In order to optimize sensitivity to Mn^{2+} enhancement while still enabling mapping of topographic organization within major brain structures, we chose to scan at a moderate isotropic resolution of 390 μm. We observed significant Mn^{2+} signal enhancement corresponding with anterograde transport in major cortical and subcortical targets within 6–10 h. The atlas-based analysis helped identify the regions containing labeling and proved useful for comparing data recorded in different experiments. A more focused 3-D analysis of Mn^{2+} signal enhancement within the thalamus demonstrated a general corticothalamic topographic organization corresponding with earlier described two-dimensional topographic schemes (Fabri and Burton, 1991).

Methods

Eight adult male Sprague-Dawley rats (230–500 g) were used for $MnCl_2$/MRI tracing. In addition, data from two previously published conventional neural tracing experiments (Leergaard et al., 2000) were included for comparative purposes. Animal procedures were approved by an institutional animal welfare committee and were in compliance with National Institutes of Health guidelines for the use and care of laboratory animals.

3-D reconstruction of the Swanson stereotaxic atlas

A 3-D digital reconstruction was created using 2-D figures from the Swanson stereotaxic atlas of the rat brain (Swanson, 1999), which is based on coronal histological sections from one adult male Sprague-Dawley rat (Swansons Figs. 1 through 50, Adobe illustrator format). The figures were aligned according to atlas stereotaxic coordinates, and the outlines of the brain surface, the corpus callossum/white matter, the ventricular system, and the boundaries of selected brain nuclei were digitized as contour lines using a modified version of the program MicroTrace (Leergaard and Bjaalie, 1995). The digitized drawings were reconstructed in 3-D using the program Micro-3D (Oslo Research Park, Oslo, Norway; cf., Bjaalie et al., 1997; Leergaard and Bjaalie, 2002). Surface modeling and tools for slicing the 3-D model at chosen thickness and angle, available in Micro3D, were used to generate "atlas" slices corresponding to slices through MRI volumes or histological sections (see below). The 3-D surface model served as a template for combining 3-D image data and 2-D section data. In the MRI volumes, measurements of anatomic landmarks, such as the anterior-posterior, mediolateral, and dorsoventral extent of the brain surface, the distance between the genu and splenium of the corpus callossum, the ventricular system, and the thickness of the cortical grey matter, served as basis for an affine transformation to fit the atlas.

Manganese-enhanced MRI tracing

Rats were anesthetized with urethane (Abbott, Chicago, IL; 1.2 g/kg ip, with 10% supplements during surgery as needed). This provided stable anesthesia for the entire imaging session (see also Field et al., 1993). Cranial surgery and tracer injection were performed as described elsewhere (Leergaard et al., 2000). Briefly, the head was positioned and immobilized in a stereotaxic frame, and a small opening was made in the skull and dura overlying the SI cortex. The presumed hindlimb or face representations in medial and anterolateral parts of SI, respectively, were identified stereotaxically according to the topographic map of Chapin and Lin (1984), and ~10 nl of an aqueous solution of 0.8 M manganese chloride ($MnCl_2$; ICN Biomedicals Inc., Aurora, OH) was slowly injected 1.0 mm below the pial surface through a glass pipette mounted on a 1.0-μl Hamilton syringe that was placed in a microinjection unit (Kopf 5001, Kopf Instruments, Tujunga, CA). The pipette was left in situ for 2 min before it was slowly retracted and removed. Animals were hydrated by intraperitoneal injection of 1.0 ml of a 5% dextrose solution prior to imaging. For MRI imaging the rat head was immobilized in a plastic stereotaxic frame. Body temperature was maintained at 37 °C by a water-circulating heating pad (Gaymar T/Pump; Gaymar Industries, Orchard Park, NY). The animals were tracheotomized, and a thin plastic tube was inserted into the tracheal tube to monitor respiratory frequency and expired CO_2

concentration using a capnograph (V9004, Harvard Apparatus, Holliston, MA). Since use of urethane is restricted to nonsurvival procedures (see, e.g., Buelke-Sam et al., 1978; Field and Lang, 1988), euthanasia was performed immediately at the end of each imaging experiment with an overdose of sodium pentobarbital (200 mg/kg).

MR images were obtained at the Massachusetts General Hospital NMR-Center using a 3 T whole-body human scanner (Siemens Medical Solutions, Iselin, NJ), using a custom-made loop surface receiver coil (8 cm diameter) centered on the intersection of the body midline and the interaural line, approximately 5 mm above the external auditory meatus. The (human) body RF coil was used to provide a uniform B_1 transmit field for excitation. Use of a large excitation coil ensured uniform contrast in T_1-weighted images. The relatively large (8 cm diameter) receive coil was chosen to provide nearly uniform reception sensitivity over the rat brain. A smaller coil (e.g., 3 or 4 cm diameter) would have provided higher sensitivity but reduced uniformity. T_1-weighted volumetric images were obtained using a 3-D FLASH sequence with TR/TE/flip angle = 20 ms/8.17 ms/25°. Images were obtained with 390 μm isotropic voxels, field of view = 50 × 50 × 50 mm, matrix = 128 × 128 × 128. The relatively large field of view was chosen to ensure that no aliasing artifacts from the rat's shoulder or paws interfered with the image. Each individual scan lasted 5 min and 29 s. The animals were scanned continuously, starting within an hour after the $MnCl_2$ injection and continuing for up to 20 h after injection. The MRI volume series were corrected for rigid body motion during the scanning sessions (Woods et al., 1998), and linear regression was performed to fit the intensity changes over time for each voxel. Mn^{2+}-labeled regions within the region of interest (identified by 3-D brain atlasing, see below) were mapped by identifying contiguous voxels in which the fitted signal increase over time was statistically significant ($P < 10^{-5}$, uncorrected for multiple comparisons).

The temporal evolution of Mn^{2+} signal enhancement in selected regions of interest (previously determined to contain significant signal increase over time, see above) was studied by measuring the intensity change over time relative to adjacent control regions in continuous time series. The change in relative signal intensity over time was fitted to an incomplete gamma function given by $g(x,\tau,a) = a\int_0^x t^2 e^{-1/\tau} dt$ using a nonlinear fitting procedure (Fig. 4). The statistical time series analysis and visualization of the results were performed using the FreeSurfer software package (freely downloadable from http://surfer.nmr.mgh.harvard.edu/), augmented by custom-designed software written in Matlab (Mathworks, Inc., Natick, MA).

The moderate resolution used for this study allowed for a large number of short scans (typically 60–100 vol per experiment) to be combined for the statistical analysis. This greatly increased the statistical power for detecting subtle signal enhancements, compared to the power that could be achieved using fewer, longer scans with higher resolution. Mn^{2+}-labeled zones within the thalamus were reconstructed in 3-D by digitizing the boundaries of the labeling from coronal section images, using the same 3-D reconstruction method as described above.

Anterograde tract tracing data

To validate the specificity of the $MnCl_2$/MRI method, we compared the distribution of Mn^{2+} signal enhancement with labeling patterns obtained with the conventional neural tracer biotinylated dextran amine (BDA). A material of two rats from a previous study (Leergaard et al., 2000) was used. In one of these animals BDA was injected medially in SI (at a location corresponding to the medial injections of $MnCl_2$), and labeled neuronal elements were investigated in 50-μm-thick coronal sections. In another animal, several injections of BDA were placed in SI, and the ensuing labeling was investigated in 50-μm-thick sagittal sections. Detailed specifications for these experiments are available in Leergaard et al. (2000, cf. cases R102 and R118). The entire 50-μm-thick sections were photographed through a Nikon Multiphot microscope (Nikon, Tokyo, Japan), equipped with a MacroNIKKOR 1:4:5 lens, and the photographs were subsequently digitized using a flatbed scanner. The correct anterioposterior position and section angle of the histological sections were determined before the section images were scaled to fit the 3-D atlas model.

Results

Manual segmentation of MRI data by three-dimensional brain atlasing

Our partial 3-D reconstruction of the Swanson atlas (Fig. 1) contained solid surface representations of the outer surface of the brain, the outer boundaries of white matter, the ventricular system, the caudate-putamen complex (Fig. 1B, pink surface), the medial and lateral segment of the globus pallidus, and the thalamic complex (as defined in Swanson, 1999; Fig.1B, green surface). Within the thalamus, the boundaries of the reticular nucleus (RT), the ventral posteromedial nucleus (VPM), ventral posterolateral nucleus (VPL), and the posterior complex of the thalamus (PO) were reconstructed. The 3-D surface model served as a template for linear scaling and spatial registration of MRI data, as well as an aid for manual segmentation of recognizable anatomic landmarks in the MRI images. In the original T_1-weighted MRI images the boundaries of the white matter and the ventricular system were readily seen (Figs. 2 and 3). Also the characteristic shapes of the hippocampus, basal ganglia, tectum, and descending corticobulbar and corticospinal fiber tracts, could be partly identified (Fig. 3). Combined visualization of MR images together with the 3-D

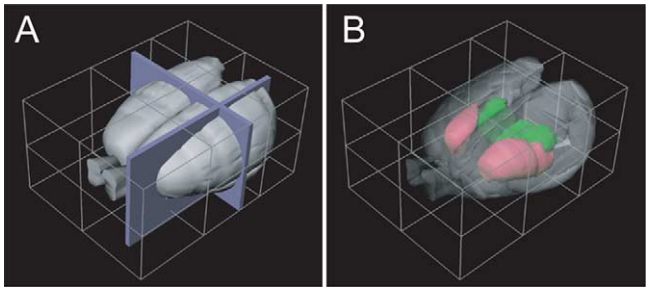

Fig. 1. Digital atlas reconstructed from serial section drawings available in the Swanson atlas of the rat brain (Swanson, 1999). In A, the reconstructed external surface is shown as a solid surface. Stereotaxic atlas coordinates are shown as a bounding box with selected reference lines. The position and orientation of the coronal and sagittal slices in Fig. 2 are shown as solid blue boxes in A. In B, the external surface is made transparent and the boundaries of the caudate-putamen complex (pink) and the thalamus (green) are seen.

surface model allowed a more reliable segmentation of the boundaries of the basal ganglia and the thalamus (Figs. 3C,F,I, and M). Since there was a high degree of correspondence between the 3-D surface model and the recognizable structures in the raw MRI images, we used the model as a basis for determining boundaries that were not identifiable in the MR images. The segmentation of anatomic landmarks was facilitated by use of customized atlas slices, obtained by subdividing the 3-D digital surface model into slices oriented to match the coronal, sagittal, and horizontal MRI slices. This was particularly helpful for distinguishing between Mn^{2+}-enhanced signals within the thalamus and in the internal capsule (Figs. 3H and I).

General features of labeling

$MnCl_2$ was injected in cortical SI regions corresponding to face representations ($n = 4$) and trunk/hindlimb representations ($n = 4$). When the animals were scanned 30–60 min after the injection, the injection sites were visible as bright regions in T_1-weighted images (Figs. 2A and C and 3A,D, and K). The high signal intensity region surrounding the point of injection typically had a radius of ~2 mm within 1 h after injection, increasing to ~4 mm after 9 to 10 h (Figs. 2 and 3). In the center of the injections, we often observed low signal intensity (Figs. 2A and B and 3D and E), presumably associated with high concentration of Mn^{2+} (see Discussion). Mn^{2+} signal enhancement was visible in the corpus callosum within 1 h after injection. After 3.5–4 h distinct intracortical signal enhancement could be seen in the ipsilateral secondary somatosensory cortex (SII), and contralateral SI (Figs. 2B and 3B), as well as in the other cortical sites. The spatial distribution of signal enhancement in the contralateral SI mirrored the central region of the injection sites (Fig. 2B). In cases where $MnCl_2$ was injected laterally in the SI (face representation), signal enhancement was observed in the ipsilateral primary motor cortex. In cases containing $MnCl_2$ injection medially in SI (trunk/hindlimb representation), corresponding (partly overlapping) representations in MI were located within the intense signal surrounding the injection site (Fig. 2D). We did not observe significant signal enhancement in the ipsilateral and contralateral perirhinal cortex, nor in the contralateral SII, which reportedly receive projections from SI (Welker et al., 1988; see also Waite and Tracey, 1995).

Subcortical signal enhancement was observed in a number of expected locations, as exemplified in Figs. 2, 3, and 5. Labeling was observed bilaterally in the caudate-putamen complex, ipsilaterally in the thalamus, internal capsule, superior colliculus, and pontine nuclei, and in the descending corticobulbar and corticospinal pathways. Signal enhancement observed in the superior colliculus and pontine nuclei was variably above or at the significance threshold used ($P < 10^{-5}$). In cases that had received $MnCl_2$ injection *medially* in SI (trunk/hindlimb representation), distinct signal enhancement was observed throughout the descending fiber tract to the level of the cervical spinal cord (Figs. 5A and C). When $MnCl_2$ was injected *laterally* in SI (face representation), signal enhancement could be followed through the medulla oblongata (Figs. 5B and D). It was not possible to detect any significant signal enhancement in the contralateral trigeminal nuclear complex, known to receive projections from SI facial representations (Wise et al., 1979; Welker et al., 1988; Killackey et al., 1989).

The time course of MRI signal intensity changes in selected cortical and subcortical target regions are shown in Fig. 4. In all regions, a brief initial time delay (i.e., with little change from the baseline intensity) was seen before the intensity values gradually increased. The accumulation of Mn^{2+} signal enhancement can be closely approximated by

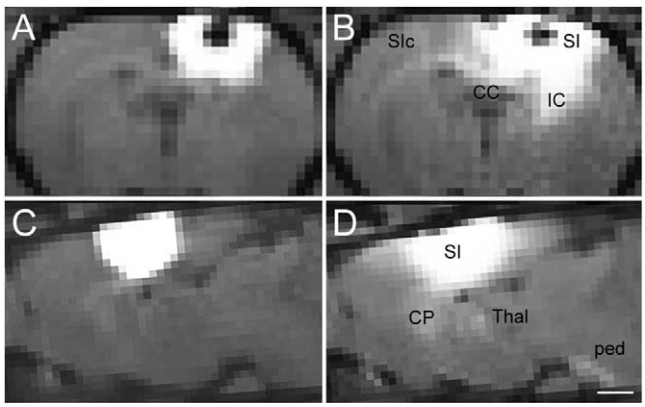

Fig. 2. Coronal (A,B) and sagittal (C,D) slices showing signal enhancement after injection of $MnCl_2$ medially in SI (hindlimb representation). A and C show the injection site ~40 min after the injection. At the point of injection a central zone of low signal intensity is visible, surrounded by a halo of bright signal enhancement. B and D show the corresponding slices ~9 h later. In B, distinct Mn^{2+} signal enhancement is apparent in the internal capsule, the corpus callosum, and the contralateral SI. In D, discrete Mn^{2+} signal enhancement is visible in the caudate-putamen, thalamus, and in the descending corticospinal and corticobulbar tract. CC, corpus callosum; CP, caudate-putamen; IC, internal capsule; Ped, peduncle; SI, primary somatosensory cortex; SIc, contralateral SI; Thal, thalamus. Bar, 2 mm.

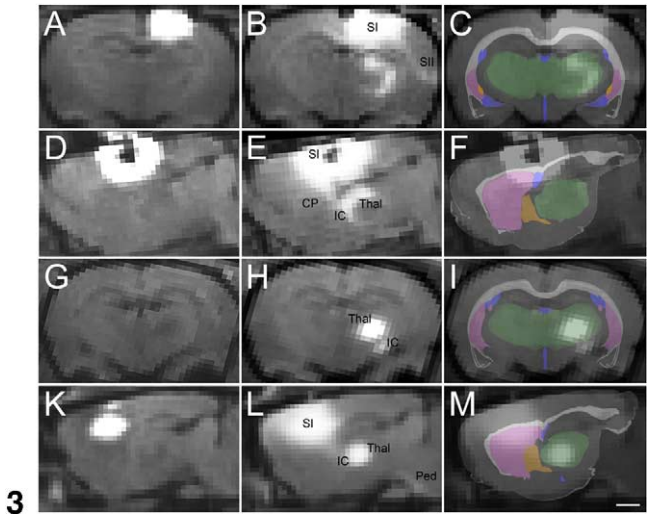

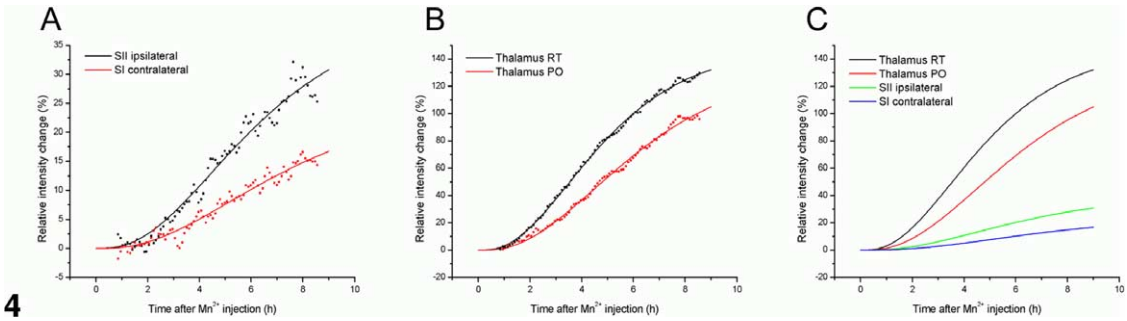

Fig. 3. Corticothalamic topography revealed by $MnCl_2$/MRI tracing. The left column (A,D,G,K) shows raw MR images acquired 40–60 min after injection of $MnCl_2$. The middle column (B,E,H,L) shows raw MR images acquired 9–10 h later, and the right column (C,F,I,M) shows the same MR images superimposed on corresponding parts of the 3-D digital atlas from Fig. 1. Data from two representative experiments are shown. In one animal (A–F), the tracer was applied to medial parts of SI (hindlimb representation, same case as shown in Figs. 2 and 5A and C). In another animal (G–M), a more lateral part of SI was injected (face representation, same case as shown in Figs. 5B and D). Injection of manganese into SI gave rise to Mn^{2+}-enhanced signals in descending corticofugal pathways (internal capsule, IC; peduncle, ped), and in multiple brain regions within 6–10 h, most notably within the caudate-putamen complex (CP), the ipsilateral secondary somatosensory cortex (SII), and the thalamus (Thal). By superimposing the MR volumes from the two cases onto the 3-D digital atlas, it was possible to delineate major brain regions within the MRI volume (bright gray, white matter; pink, caudate-putamen; orange, globus pallidum; green, thalamus), and to demonstrate across animal topographic differences. Bar, 2 mm.

Fig. 4. Time course of MRI signal changes in selected cortical and subcortial regions after injection of $MnCl_2$ in SI trunk/hindlimb representation (same case as shown in Figs. 2, 3A–F, and 5A and C). Signal intensity measurements were obtained from several contiguous voxels in regions containing significant Mn^{2+} signal enhancement and corresponding adjacent control regions. The ordinate shows normalized signal intensities expressed as percentage change from baseline, after subtraction of mean percentage signal changes in the corresponding control regions. Data are shown as scatter plots and as lines fitted to a sigmoid function. A and B show the time course of intensity changes in two cortical (ipsilateral SII and contralateral SI) and subcortical (reticular nucleus thalamus and posterior complex thalamus) target regions, respectively. C shows a comparison of the sigmoid fitted curves shown in A and B. Signal intensities are initially close to baseline before gradually increasing.

a sigmoidal curve (incomplete gamma function; ipsilateral SII, $R^2 = 0.96$, $\tau = 2.2 \pm 0.17$; contralateral SI, $R^2 = 0.96$, $\tau = 2.55 \pm 0.26$; reticular nucleus thalamus, $R^2 = 0.99$, $\tau = 2.22 \pm 0.06$; posterior complex thalamus, $R^2 = 0.99$, $\tau = 1.72 \pm 0.02$; see also Fig. 4).

The time at which Mn^{2+} signal enhancement was first seen (i.e., reached signal intensities just above the detection threshold of our experimental setup) in different cortical and subcortical regions was to some extent related to the distance from the injection site (measured along the axonal trajectories, below referred to as "distance"). For example, in one case (receiving $MnCl_2$ injection in SI trunk/hindlimb representation) distinct signal enhancement was seen in target regions (gray matter) after 1 h in the reticular nucleus thalamus (distance ~4.5 mm), after 2 h in the posterior complex thalamus (distance ~6 mm), and after 3.5 h in the ipsilateral SII (distance ~7.5 mm) and contralateral SI (distance ~8 mm). In corticofugal pathways (white matter) Mn^{2+} signal enhancement was observed after 40 min in the internal capsule (distance ~4 mm), after 1.5 h in the cerebral peduncle at level of the mesencephalon (distance ~7 mm), after 2.5 h in the cerebral peduncle at level of the pons (distance ~13 mm), after 3 h in the cerebral peduncle at level of the inferior olive (distance ~16 mm), and after 4 h in the pyramidal decussation (distance ~22 mm). Given the gradual signal buildup observed in all the inspected regions,

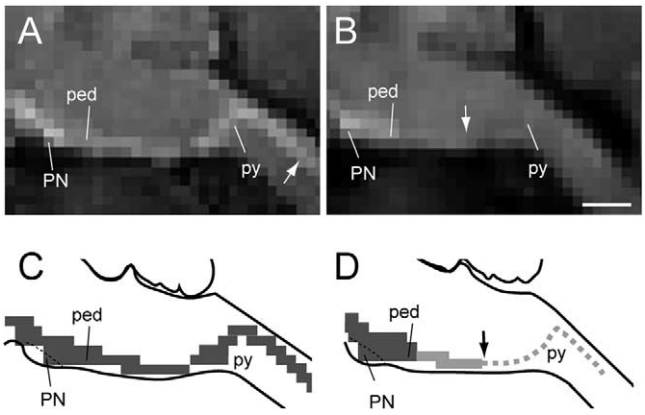

Fig. 5. Mn^{2+} enhancement in corticobulbar and corticospinal pathways. A and B show maximum intensity projections of 2.4-mm-thick MRI slabs from two representative animals, and C and D show schematic interpretations of the same images. In one animal (A, C), the tracer was applied to medial parts of SI (hindlimb representation). In another animal (B, D), the tracer was injected more laterally in SI (face representation). In A and C, significant signal enhancement is seen in the entire trajectory of the corticobulbar and corticospinal tract, through the pyramidal decussation (py) into the cervical spinal cord (arrow in A). In B, significant signal enhancement could be followed to the medulla oblongata (arrow in B and D). In this case, the signal enhancement in the medulla oblongata (indicated with brighter shade of gray in D) was significant, close to the significance threshold ($P = 10^{-5}$). In caudal parts of the medulla oblongata and in the cervical spinal cord, only weak (nonsignificant) signal enhancement was observed (dotted gray line in D). In both cases, signal enhancement is seen in the pontine nuclei (PN). Bar, 1 mm.

it is clear that the time required to reach a given detection threshold critically depends on the sensitivity of the imaging technique used, and also by the density of axonal projections. It is therefore difficult to obtain definitive estimates of transport rates from such observations (see Discussion).

To validate the specificity of the $MnCl_2$/MRI method, the distribution of Mn^{2+} signal was compared to histological material obtained from comparable experiments using the conventional neural tracer BDA (from Leergaard et al., 2000). The two data types were coregistered with use of the 3-D surface model. As observed in a single coronal section through the thalamus (Fig. 6A), delineated and restricted axonal labeling was visible in the ipsilateral SII, in the contralateral SI, and within the VPM and PO after a single injection of BDA in medial parts of SI (Fig. 6A). The overall distribution of BDA labeling in this section corresponded well with the observed Mn^{2+} signal enhancement in cases that had received $MnCl_2$ injections medially in SI, although the extent of Mn^{2+} signal enhancement within the thalamus appeared more extensive (Fig. 3B). A small difference in the location within SI of the Mn^{2+} and BDA injections corresponded with a shift of the distribution of labeling in the ipsilateral SII (compare Figs. 3B and 6A). Further, SI-thalamic BDA labeling in a sagittal section corresponded well with the pattern of signal enhancement observed in the RT, VPM, and VPL following Mn^{2+} injection in SI (compare Figs. 3E and 6B).

Gross 3-D anatomy of SI corticothalamic pathways

We explored in further detail topographic differences in the distribution of Mn^{2+} signal enhancement arising in medial and lateral parts of SI, respectively. Comparison of corresponding coronal and sagittal slices through the thalamus in two representative experiments showed that labeling originating in medial parts of SI (Figs. 3B,C,E, and F; hindlimb/trunk representation) occupied a more external location than labeling originating more laterally in SI (Figs. 3H,I,L, and M; face representation). This topographic inside-out shift in distribution is clearly demonstrated in the pseudo-colored combinations of the images (Figs. 7C and D). To better visualize the large-scale 3-D topography of these corticothalamic projections, the outer boundaries of Mn^{2+}-labeled zones in the thalamus were 3-D reconstructed and shown in registration with the 3-D surface model (Figs. 7A,B and F). The two labeled volumes involved several thalamic subnuclei and overlapped considerably. Nevertheless, a topographic distribution was observed. By slicing the combined reconstructions of the thalamus and the Mn^{2+}-labeling patterns in three coronal and two sagittal slices (Fig. 7B), we found that the volume of the thalamus which received input from medial parts of SI (trunk/hindlimb representations) was located outside (i.e., more medially, ventrally, and laterally) than the thalamic volume receiving projections from lateral parts of SI (facial representations). A mid-thalamic slice through the 3-D reconstructions clearly showed a topographic organization with medial parts of SI projecting predominantly to lateral parts of PO and VPL (Fig. 7F, yellow), and lateral parts of SI projecting to more medial parts of PO and VPM (Fig. 7F, red). Overlap between the two projections was predominantly observed in

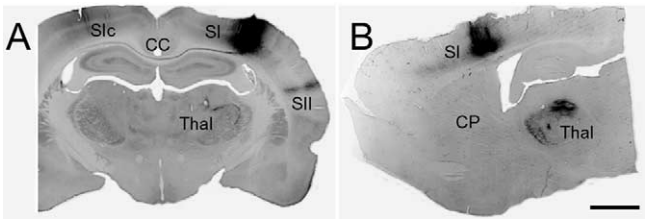

Fig. 6. Results from conventional tracing experiments to be compared with Mn^{2+}/MRI data in Fig. 3. Topographic organization in the corticothalamic pathways is revealed by single (A) and multiple (B) injections of biotinylated dextran amine (BDA) into the SI cortex. A shows a coronal section through the cerebral cortex following a single injection of BDA medially in SI. The distribution of BDA labeling in this section should be compared with the Mn^{2+}/MRI tracing data in Figs. 2B and 3B. Both methods gave rise to labeling in the secondary somatosensory cortex (SII), the corpus callosum (CC), contralateral SI (cSI), and thalamus (Thal). Corticothalamic labeling is more restricted in sections with BDA labeling than in the Mn^{2+}/MR image. The image in B shows a sagittal section through the cerebral cortex following several injections of BDA into SI (only a limited part of the BDA-injected region is visible in this section). In this case, a large zone of corticothalamic labeling was visible. This labeling pattern corresponded well with the corticothalamic Mn^{2+}/MRI labeling in Fig. 2C. Bar, 2 mm.

the parts of PO, VPL, VPM, and RT that corresponded to regions containing fibers en route to their target (Deschenes et al., 1994; Deschenes et al., 1998; Alloway et al., 1999; Figs. 3 and 7). Our 3-D $MnCl_2$/MRI tracing data corresponded well to the overall scheme of reciprocal corticothalamic connectivity reported with the use of conventional tracing methods in single sections by Fabri and Burton (Fig 7E; Fabri and Burton, 1991; for reviews, see, e.g., Deschenes et al., 1998; Price, 1995).

Discussion

In this study, we demonstrate that the MRI detectable T_1 contrast agent $MnCl_2$ is suitable for rapid in vivo anterograde tracing of major corticocortical and cortico-subcortical projections in the rat. Focal injections of $MnCl_2$ into somatosensory cortex gave rise to topographically specific Mn^{2+} signal enhancement at expected locations within the ipsilateral and contralateral cerebral cortex, as well as in corticostriatal, corticothalamic, corticotectal, corticopontine, and corticospinal pathways. We advance the $MnCl_2$/MRI technique to visualize topographic organization in the central nervous system by spatial coregistration of MRI data with a 3-D reconstruction based on a standard stereotaxic atlas. Linear registration of MRI volumes with the 3-D model allowed across-animal comparison and visualization of known topographic organization in corticothalamic pathways. We show that a commonly available 3 T human scanner represents an adequate entry level for this type of investigation.

Identification of anatomic landmarks in MR images is variably difficult depending on the employed scanning resolution and parameters. In our T_1-weighted images, with relatively poor structural contrast, the use of linear scaling techniques for spatial registration of MRI volumes with a template 3-D reconstruction of the Swanson atlas (Swanson, 1999) was particularly helpful for assessing the boundaries of several subcortical structures, and for assigning localization to the observed labeling patterns within the thalamus. The linear registration of the MR images with the atlas reconstruction was achieved by matching well-known anatomic structures, readily recognized in the MR images, such as the outer boundaries of the brain, the white matter, and the ventricular system. The accuracy of the spatial registration was subsequently validated by slice-by-slice comparison of multiple structures in atlas and image volumes at different angles of view. The rat brain, with a considerably smaller individual variability compared to brains of higher mammals, is particularly suited for affine registration procedures (for reviews, see Ashburner and Friston, 1999; Bjaalie, 2002). The 3-D surface model allowed us to prepare customized atlas slices with the same orientation as the coronal, sagittal, and horizontal MRI slices, and further provided a framework for combining data from individual experiments. This was fundamental for the investigation of topographical organization in the present study.

A neural tracer can only provide useful results if the location and approximate size of the effective injection site can be determined (for general discussions, see, e.g., Mesulam, 1982; Wouterlood and Groenewegen, 1991). In the present material, the center of the injection sites could often be identified as a zone of low signal intensity (Figs. 2A and B). This may be explained by T_2* intravoxel dephasing from the magnetic susceptibility associated with high Mn^{2+} concentration. (Although our images are primarily T_1 weighted, at TE = 8.17 ms, the extreme susceptibility of the concentrated Mn^{2+} at the injection site will cause significant intravoxel dephasing.) Around this central core of low signal intensity, a halo of bright Mn^{2+} signal enhancement, with decreasing peripheral intensity, developed over time (Figs. 2 and 3). This extensive signal enhancement may be caused by local axonal transport or extracellular diffusion of Mn^{2+}. Presuming that the diffusion coefficient of Mn^{2+} is similar to the apparent diffusion coefficient reported for extracellular diffusion of water in cortical tissue slices (Nicholson and Sykova, 1998), we estimate that Mn^{2+} can diffuse as much as 2 mm away from the point of injection within the first hour after injection and up to ~6 mm after 10 h. (In our material, the halo extends only ~4 mm from the injection center at 10 h.) We are inclined to believe, however, that the effective injection site extends only into a limited part of this halo, since labeling in contralateral SI mirrors primarily the central core region of the injection site (Fig. 2B) and not the surrounding halo (for references to reciprocal SI–SI projections; cf. Welker et al., 1988; Waite and Tracey, 1995). The finding of precise and restricted labeling in the ipsilateral SII (Fig. 3B) further supports this notion. The relatively extensive corticothalamic labeling (Fig. 3), and the large amount of overlap (Fig. 7), could correspond to uptake of tracer from a relatively wide region of the SI cortex. On the other hand, the relatively large voxel size used in the present experiments, and labeled fibers traversing the thalamus en route to different subnuclei (Deschenes et al., 1994, 1998; Alloway et al., 1999), could well explain the extensive and overlapping labeling observed in the thalamus.

All labeling obtained in our study can be explained by direct projections from the injection site. Previous reports using longer survival periods reported evidence for transsynaptic transport (Pautler et al., 1998; Saleem et al., 2002; Takeda et al., 1998; Henriksson et al., 1999). The $MnCl_2$/MRI technique as applied here allowed visualization of major projection pathways from a given SI injection site. With our experimental setup, and within the timeframe of our experiments, the method was not sensitive enough to map the "complete" projection trajectories known from conventional tracing studies. While SI projections to ipsilateral SII, MI, and contralateral SI were readily detected, known bilateral projections to the perirhinal cortex and contralateral SII (Welker et al., 1988) were not demonstrated. Nei-

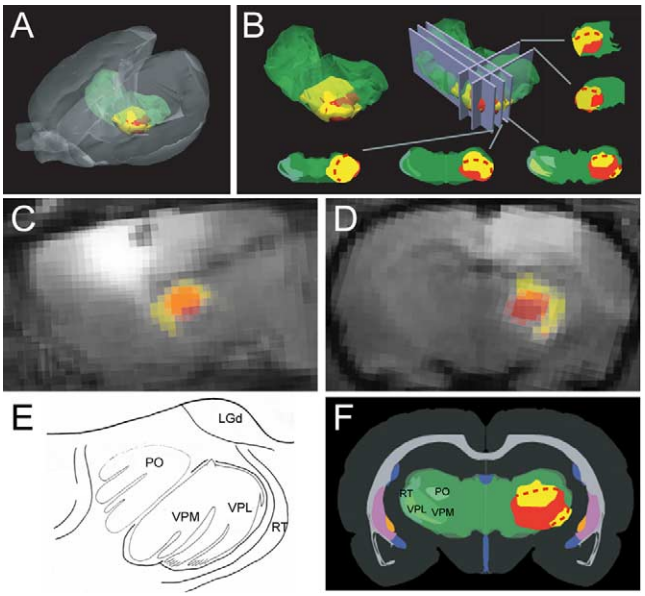

Fig. 7. A 3-D reconstruction of the signal enhancement patterns obtained with Mn^{2+}/MRI tracing experiments, warped into the 3-D reconstruction of the Swanson brain atlas. A shows the surface representations of the corticothalamic projections from medial (hindlimb, yellow) and lateral (face, red) parts of SI, in registration with the 3-D surface model. B shows the use of slicing at different angles through the reconstruction to investigate topographical labeling patterns. C and D show pseudo-colored combinations of the images shown in Figs 3B and E and H and L, respectively. The superimposed images in C and D demonstrate the inside-out shift in the topography of projections originating in the lateral and medial parts of SI, respectively. E shows the reciprocal topographical organization scheme of corticothalamic and thalamocortical projections (modified from Fabri and Burton, 1991, with permission), which corresponded well with the results of the present study, summarized in F. The contralateral counterparts of the thalamic subnuclei used for assigning location to corticothalamic labeling are shown in shades of green in B and F. LGd, lateral geniculate complex, dorsal part; PO, posterior complex thalamus; RT, reticular nucleus thalamus; VPM, ventral posteromedial nucleus thalamus; VPL, ventral posterolateral nucleus thalamus.

ther was it possible to visualize known corticotrigeminal projections (Wise et al., 1979; Welker et al., 1988; Killackey et al., 1989) from the lateral parts of SI. This might be explained by threshold effects caused by voxel size and the signal-to-noise ratio in the MR images, as well as by a more diffuse and quantitatively smaller nature of these pathways.

A higher spatial resolution would have been desired in order to discern topographic organization within, e.g., the superior colliculus and pontine nuclei (see, e.g., pontine nuclei in Fig. 5). However, while it is possible to detect Mn^{2+} signal enhancement with higher spatial resolution than used here (Lin et al, 2001; Watanabe et al., 2001; Pautler and Koretsky, 2002), the resulting signal-to-noise ratio (SNR) is dramatically reduced. Specifically, since the signal is proportional to the voxel volume, the use of 200 μm isotropic voxels would result in a reduction of the SNR by a factor of 8 (for the same scan time) compared to that obtained in the present study, using 390 μm isotropic voxels. Consequently, a 64-fold increase in scan time would be required to obtain equivalent sensitivity. Some improvement can be achieved by scanning with higher field strength, although the signal-to-noise improvement is at best proportional to field strength (Haacke et al., 1999). Since the purpose of the present study was to perform a global mapping of cortical and subcortical projections, we gave priority to sensitivity to signal enhancement over spatial specificity.

Analysis of the temporal evolution of Mn^{2+} signal enhancement in selected regions of interest shows sigmoid-shaped increase in signal intensity over time (Fig. 4). During the first 1–3 h of the experiment signal intensities in known target regions are relatively close to baseline. This is consistent with a pure delay of 1–3 h reflecting the time required for uptake at the injection site and axonal transport, followed by gradual accumulation of Mn^{2+}. The rate of signal accumulation at a target location would be expected to depend on the density of projections, the uptake rate of Mn^{2+} at the injection site, and the transport and/or diffusion away from the target location. Previous studies have obtained estimates of the speed of Mn^{2+} transport by dividing the distance from the center of the injection site to the structures of interest by the time delay before Mn^{2+} signal enhancement is first detected (Van der Linden et al., 2002). Applying the same method to our material, Mn^{2+} transport rates could be estimated to 2.1–2.6 mm/h in different cortical and subcortical target regions (SI, SII, thalamus, and pontine nuclei), and to 4.6–6.1 mm/h in descending corticofugal pathways (between the internal capsule and the pyramidal decussation). These rates are well within the previously established range of fast axonal transport (2–16 mm/h, Jacob and O'Donoghue, 1995; Elluru et al., 1995; Brown, 2003) and broadly consistent with those reported by others (2 mm/h, Pautler et al., 1998; 2.8 mm/h, Watanabe et al., 2001; 1.14–1.42 mm/h, Saleem et al., 2002; 2–6 mm/h, Van der Linden et al., 2002). However, since the time interval used for calculation also includes the time needed for Mn^{2+} uptake, transport, and accumulation in the target area, we believe that the reported Mn^{2+} transport rates are underestimates. It should also be noted that the transport rate estimates obtained using this approach depend critically on the sensitivity of the employed experimental setup as well as the density of axonal projections onto a target region. Further investigations will be needed to quantitatively model the Mn^{2+} signal kinetics, including diffusion, uptake, and transport. Meanwhile, the above given estimates may serve as guidelines for expected time for detection of Mn^{2+} signal enhancement with a given experimental setup.

We show that it is possible to use Mn^{2+}-enhanced MRI tracing techniques to demonstrate large-scale topographic organization in somatosensory pathways in small animals using commonly available 3 T clinical MRI scanners. Data acquisition is much more efficient with the $MnCl_2$/MRI technique than with conventional histological, section-based techniques. The method thus opens avenues for rapid

and simultaneous 3-D analysis of multiple brain regions and whole brain. One use of the method could be to compare overall anatomical organization in groups of animals submitted to different external or genetic perturbations. Finally, since this in vivo neural tracing technique also will allow longitudinal anatomic investigations, another potential advantage will be analysis of plasticity and regeneration in neural pathways, with individual animals serving as their own controls.

Acknowledgments

Financial support was provided by The Research Council of Norway and General Tønder Bull og hustrus legat to T.B.L., European Community Grant QLRT-2000-02256 to J.G.B., and grants from the MIND Institute and NIH (R01-EB00790, R01-EB00307, and R01-NS39581) to A.M.D. We thank Per Andersen for critical comments to the manuscript, David Boas for lending access to his laboratory, and Doug Greve, Carina Knudsen, Andre Van der Kouwe, Christian Pettersen, Kevin Teich, and Andreas Potthast, for expert technical assistance.

References

Alloway, K.D., Crist, J., Mutic, J.J., Roy, S.A., 1999. Corticostriatal projections from rat barrel cortex have an anisotropic organization that correlates with vibrissal whisking behavior. J. Neurosci. 19, 10908–10922.

Ashburner, J, Friston, K.J., 1999. Spatial Normalization, in: Toga, A.W. (Ed.), Brain Warping. Academic Press, San Diego, pp 27–44.

Bjaalie, J.G., 2002. Localization in the brain: new solutions emerging. Nature Neurosci. Rev. 3, 322–325.

Bjaalie, J.G., Daehlen, M., Stensby, T.V., 1997. Surface modelling from biomedical data. in: Daehlen, M, Tveito, A. (Eds.), Numerical Methods and Software Tools in Industrial Mathematics. Birkhauser, Boston, pp 9–26.

Brodal, A., 1981. Neurological Anatomy in Relation to Clinical Medicine. Oxford Univ. Press, Oxford.

Brown, A., 2003. Axonal transport of membranous and nonmembranous cargoes: a unified perspective. J. Cell Biol. 160, 817–821.

Buelke-Sam, J., Holson, J.F., Bazare, J.J., Young, J.F., 1978. Comparative stability of physiological parameters during sustained anesthesia in rats. Lab. Anim. Sci. 28, 157–162.

Chapin, J.K., Lin, C.S., 1984. Mapping the body representation in the SI cortex of anesthetized and awake rats. J. Comp. Neurol. 229, 199–213.

Cowan, W.M., Cuénod, M., 1975. The Use of Axonal Transport for Studies of Neuronal Connectivity. Elsevier, Amsterdam.

Deschenes, M., Bourassa, J., Pinault, D., 1994. Corticothalamic projectionsfrom layer V cells in rat are collaterals of long-range corticofugal axons. Brain Res. 664, 215–219.

Deschenes, M., Veinante, P., Zhang, Z.W., 1998. The organization of corticothalamic projections: reciprocity versus parity. Brain Res. Brain Res. Rev. 28, 286–308.

Elluru, R.G., Bloom, G.S., Brady, S.T., 1995. Fast axonal transport of kinesin in the rat visual system: functionality of kinesin heavy chain isoforms. Mol. Biol. Cell 6, 21–40.

Fabri, M., Burton, H., 1991. Topography of connections between primary somatosensory cortex and posterior complex in rat: a multiple fluorescent tracer study. Brain Res. 538, 351–357.

Field, K.J., Lang, C.M., 1988. Hazards of urethane (ethyl carbamate): a review of the literature. Lab. Anim. 22, 255–262.

Field, K.J., White, W.J., Lang, C.M., 1993. Anaesthetic effects of chloral hydrate, pentobarbitone and urethane in adult male rats. Lab. Anim. 27, 258–269.

Haacke, E.M., Brown, R.W., Thompson, M.R., Venkatesan, R., 1999. Magnetic Resonance Imaging: Physical Principles and Sequence Design. Wiley, New York.

Heimer, L., Zaborszky, L., 1989. Neuroanatomical Tract-Tracing Methods 2. Recent Progress. Plenum, New York.

Henriksson, J., Tallkvist, J., Tjalve, H., 1999. Transport of manganese via the olfactory pathway in rats: dosage dependency of the uptake and subcellular distribution of the metal in the olfactory epithelium and the brain. Toxicol. Appl. Pharmacol. 156, 119–128.

Jacob, J.M., O'Donoghue, D.L., 1995. Direct measurement of fast axonal transport rates in corticospinal axons of the adult rat. Neurosci. Lett. 197, 17–20.

Killackey, H.P., Koralek, K.A., Chiaia, N.L., Rhodes, R.W., 1989. Laminar and areal differences in the origin of the subcortical projection neurons of the rat somatosensory cortex. J. Comp. Neurol. 282, 428–445.

Köbbert, C., Apps, R., Bechmann, I., Lanciego, J.L., Mey, J., Thanos, S., 2000. Current concepts in neuroanatomical tracing. Prog. Neurobiol. 62, 327–351.

Lanciego, J.L., Wouterlood, F.G., 2000. Neuroanatomical tract-tracing methods beyond 2000: what's now and next. J. Neurosci. Methods 103, 1–2.

Leergaard, T.B., Bjaalie, J.G., 1995. Semi-automatic data acquisition for quantitative neuroanatomy. Micro Trace—computer programme for recording of the spatial distribution of neuronal populations. Neurosci. Res. 22, 231–243.

Leergaard, T.B., Bjaalie, J.G., 2002. Architecture of sensory map transformations: axonal tracing in combination with 3-D reconstruction, geometric modeling, and quantitative analyses. in: Ascoli, G. (Ed.), Computational Neuroanatomy: Principles and Methods. Humana Press, Totowa, NJ, pp. 119–217.

Leergaard, T.B., Lyngstad, K.A., Thompson, J.H., Taeymans, S., Vos, B.P., De Schutter, E., Bower, J.M., Bjaalie, J.G., 2000. Rat somatosensory cerebropontocerebellar pathways: spatial relationships of the somatotopic map of the primary somatosensory cortex are preserved in a three-dimensional clustered pontine map. J. Comp. Neurol. 422, 246–266.

Lin, C.P., Tseng, W.Y., Cheng, H.C., Chen, J.H., 2001. Validation of diffusion tensor magnetic resonance axonal fiber imaging with registered manganese-enhanced optic tracts. NeuroImage 14, 1035–1047.

Mesulam, M.-M., 1982. Principles of horseradish peroxidase neurohistochemistry and their applications for tracing neural pathways—axonal transport, enzyme histochemistry and light microscopic analysis, in: Mesulam, M.-M. (Ed.), Tracing Neural Connections with Horseradish Peroxidase. Wiley, Chichester, pp 1–151.

Natt, O., Watanabe, T., Boretius, S., Radulovic, J., Frahm, J., Michaelis, T., 2002. High-resolution 3D MRI of mouse brain reveals small cerebral structures in vivo. J. Neurosci. Methods 120, 203–209.

Nicholson, C., Sykova, E., 1998. Extracellular space structure revealed by diffusion analysis. Trends Neurosci. 21, 207–215.

Pautler, R.G., Koretsky, A.P., 2002. Tracing odor-induced activation in the olfactory bulbs of mice using manganese-enhanced magnetic resonance imaging. NeuroImage 16, 441–448.

Pautler, R.G., Silva, A.C., Koretsky, A.P., 1998. In vivo neuronal tract tracing using manganese-enhanced magnetic resonance imaging. Magn. Reson. Med. 40, 740–748.

Price, J.L., 1995. Thalamus. in: Paxinos, G. (Ed.), The Rat Nervous System. Academic Press, San Diego, pp 629–648.

Saleem, K.S., Pauls, J.M., Augath, M., Trinath, T., Prause, B.A., Hashikawa, T., Logothetis, N.K., 2002. Magnetic resonance imaging of neuronal connections in the macaque monkey. Neuron 34, 685–700.

Swanson, L.W., 1999. Brain Maps: Structure of the Rat Brain. Elsevier, Amsterdam.

Takeda, A., Kodama, Y., Ishiwatari, S., Okada, S., 1998. Manganese transport in the neural circuit of rat CNS. Brain Res. Bull. 45, 149–152.

Toga, A.W., Mazziotta, J.C., 2000. Brain Mapping. The Systems. Academic Press, San Diego.

Toga, A.W., Mazziotta, J.C., 2002. Brain Mapping. The Methods. Academic Press, San Diego.

Van der Linden, A., Verhoye, M., Van Meir, V., Tindemans, I., Eens, M., Absil, P., Balthazart, J., 2002. In vivo manganese-enhanced magnetic resonance imaging reveals connections and functional properties of the songbird vocal control system. Neuroscience 112, 467–474.

Waite, P.M., Tracey, D.J., 1995. Trigeminal sensory system. in: Paxinos, G. (Ed.), The Rat Nervous System. Academic Press, San Diego, pp. 705–725.

Watanabe, T., Michaelis, T., Frahm, J., 2001. Mapping of retinal projections in the living rat using high-resolution 3D gradient-echo MRI with Mn2+-induced contrast. Magn. Reson. Med. 46, 424–429.

Welker, E., Hoogland, P.V., Van der Loos, H., 1988. Organization of feedback and feedforward projections of the barrel cortex: a PHA-L study in the mouse. Exp. Brain Res. 73, 411–435.

Wise, S.P., Murray, E.A., Coulter, J.D., 1979. Somatotopic organization of corticospinal and corticotrigeminal neurons in the rat. Neuroscience 4, 65–78.

Woods, R.P., Grafton, S.T., Watson, J.D., Sicotte, N.L., Mazziotta, J.C., 1998. Automated image registration. II, Intersubject validation of linear and nonlinear models. Assist. Tomogr. 22, 153–165.

Wouterlood, F.G., Groenewegen, H.J., 1991. The Phaseolus vulgaris-leucoagglutinin tracing technique for the study of neuronal connections. Prog. Histochem. Cytochem. 22, 1–78.